frontiers | Frontiers in Physics

ORIGINAL RESEARCH
published: 13 July 2022
doi: 10.3389/fphy.2022.910818

Dynamics of Rotating Spin-Orbit-Coupled Spin-1 Bose-Einstein Condensates With In-Plane Gradient Magnetic Field in an Anharmonic Trap

Hui Yang, Qing Zhang and Zaihe Jian*

Department of Physics, Xinzhou Teachers University, Xinzhou, China

We investigate the dynamics of rotating spin-orbit-coupled spin-1 Bose–Einstein condensates (BECs) in an in-plane gradient magnetic field, which is confined in an anharmonic trap. In the case of rotating spin-orbit-coupled spin-1 BECs with given parameters, the system evolves from initial disk-shaped condensates into drastic turbulent oscillations and ghost vortices on the surface of the component densities due to surface wave excitations and then into two final vortex necklaces along the azimuthal direction with an irregular density hole, in which the vortices differ by one quantum number in turn. For the case of rotating spin-orbit-coupled spin-1 BECs with in-plane gradient magnetic field, with the dynamic evolution, the system undergoes a transition from an initial central polar-core vortex to violent turbulent oscillations and then to a final vortex chain along the diagonal of BECs, with the remaining vortices symmetrically distributed on both sides in the individual component. In addition, the corresponding spin texture undergoes a transition from plane-wave phase to double half-antiskyrmion necklaces for the former case and a transition from a structure similar to a quadrupole magnetic field to a half-antiskyrmion chain with the rest of the half-antiskyrmions on both sides. During the dynamic evolution process, the angular momentum increases gradually and then approaches a convergent value.

Keywords: spin-orbit-coupled Bose-Einstein condensates, Anharmonic trap, dynamics, vortex, skyrmion

OPEN ACCESS

Edited by:
Lauro Tomio,
Sao Paulo State University, Brazil

Reviewed by:
Charles Reichhardt,
Los Alamos National Laboratory (DOE), United States
Farhad Sattari,
University of Mohaghegh Ardabili, Iran

****Correspondence:***
Hui Yang
yanghui20032002@163.com

Specialty section:
This article was submitted to Condensed Matter Physics, a section of the journal Frontiers in Physics

Received: *01 April 2022*
Accepted: *06 June 2022*
Published: *13 July 2022*

Citation:
Yang H, Zhang Q and Jian Z (2022) Dynamics of Rotating Spin-Orbit-Coupled Spin-1 Bose-Einstein Condensates With In-Plane Gradient Magnetic Field in an Anharmonic Trap. Front. Phys. 10:910818. doi: 10.3389/fphy.2022.910818

1 INTRODUCTION

Spin-orbit coupling (SOC) in ultracold atomic gases has been realized experimentally in the last decade [1–3], which has greatly stimulated people's interest in the study of spin-orbit-coupled quantum gases [4–6]. This new and controllable artificial SOC not only offers new possibilities for quantum simulations of spin quantum Hall effect [7, 8], topological insulators [9], and topological superconductors [10] but also provides a new direction for exploring exotic quantum phenomena, novel states of matter in the fields of ultracold atomic, molecular physics, and condensed matter physics [11–18].

A novel anharmonic trap (a harmonic trap with a quartic distortion) [19, 20], which confines the Bose–Einstein condensates (BECs) even if the rotation frequency exceeds the trapping frequency, has attracted great attention both in theory and experiment. Most research so far focuses on the ground-

state properties of BECs in an anharmonic trap [20, 21], but there are few studies on the dynamics of BECs. In this work, we investigate the dynamics of rotating spin-orbit-coupled spin-1 BECs with an in-plane gradient magnetic field in an anharmonic trap. Our research can not only obtain the stable structures of the system but also survey the detailed physical process and interesting dynamic properties of the system from an initial quantum state to a non-equilibrium state evolution and then to a final equilibrium state, which provides a new direction for exploring quantum phenomena of spin-orbit-coupled BECs in an anharmonic trap. As a matter of fact, the interesting physical properties in dynamics of quantum systems have attracted considerable interest, which includes Zitterbewegung oscillation in quenched spin–orbit-coupled BECs [22] and dynamical phases in a quenched spin–orbit-coupled degenerate Fermi gas [23].

The study is organized as follows. The theoretical model is introduced in **Section 2**. In **Section 3**, we analyze and discuss the simulation results. Finally, we summarize our findings in **Section 4**.

2 MODEL

We consider a quasi-two-dimensional (quasi-2D) spin-orbit-coupled $F = 1$ spinor BECs with an in-plane gradient magnetic field in an anharmonic trap. In the mean-field framework, the dynamics of the system can be given by the dissipative Gross–Pitaevskii (GP) form [24–27].

$$(i-\gamma)\hbar\frac{\partial\Psi}{\partial t} = H\Psi. \tag{1}$$

Here, γ is the dissipation parameter. The model is a variation and generalization of that in BECs [24, 25, 28]. In addition, this model enables one not only to find the steady state of a rotating system but also to study the whole dynamical process toward the final steady state. Moreover, this model has considered the inevitable dissipation effects in actual cold atom experiments. When we switch off the dissipation term, the simulation based on the time-dependent GP equations shows that no steady state exists. In **Equation 1**, the Hamiltonian of the system can be written as $H = H_0 + H_{\rm int}$ with

$$\begin{aligned} H_0 &= \int d\mathbf{r}\Psi^{+}\left(-\frac{\hbar^2\nabla^2}{2m} + V(\mathbf{r}) + v_{so} - \Omega L_z + g_F\mu_B\mathbf{B}(\mathbf{r})\cdot\mathbf{f}\right)\Psi, \\ H_{int} &= \int d\mathbf{r}\left(\frac{c_0}{2}n^2 + \frac{c_2}{2}|\mathbf{F}|^2\right), \end{aligned} \tag{2}$$

where $\Psi = (\Psi_1, \Psi_0, \Psi_{-1})^T$ is the order parameter normalized with the total particle number $N = \int d\mathbf{r}\Psi^{\dagger}\Psi$. m is the atomic mass, $n = n_1 + n_0 + n_{-1} = \sum_j \Psi_j^{*}\Psi_j$ $(j = 0, \pm 1)$ is the total particle density, and $\boldsymbol{r} = (x, y)$. Ω is the rotation frequency along the z -direction, and $L_z = i\hbar(y\partial_x - x\partial_y)$ denotes the z component of the angular momentum operator. The coupling constants $c_0 = 4\pi\hbar^2(2a_2 + a_0)/3m$ and $c_2 = 4\pi\hbar^2(a_2 - a_0)/3m$ represent the strengths of density–density and spin–exchange interactions, respectively. They are given in terms of the corresponding s-wave scattering length a_F for atom pairs with total spin-F. The spin density vector $\mathbf{F} = (F_x, F_y, F_z)$ is defined by $F_\alpha(\mathbf{r}) = \Psi^{\dagger}f_\alpha\Psi(\alpha = x, y, z)$, and $\mathbf{f} = (f_x, f_y, f_z)$ is the vector of the 3×3 spin-1 matrices given in the irreducible representation [29, 30]. $g_F = -1/2$ is Lande factor, μ_B denotes Bohr magnetic moment, and the in-plane gradient magnetic field (that is, the in-plane quadrupole field) $\mathbf{B}(\mathbf{r})$ is given by $\mathbf{B}(\mathbf{r}) = B(x\mathbf{e}_x - y\mathbf{e}_y)$, with B being the strength of the magnetic field gradient. Here, we choose the Rashba-type SOC, which is given by $v_{so} = k(f_x p_x + f_y p_y)$. The anharmonic trap is given by [19, 20].

$$V(r) = \frac{1}{2}m\omega_{\perp}^2\left(r^2 + \mu\frac{r^4}{a_0^2}\right) = \frac{1}{2}\hbar\omega_{\perp}\left(\frac{r^2}{a_0^2} + \mu\frac{r^4}{a_0^4}\right), \tag{3}$$

where $\omega_{\perp}$ is the radial trap frequency and $r = \sqrt{x^2 + y^2}$, $a_0 = \sqrt{\hbar/m\omega_{\perp}}$, and μ is a dimensionless constant that characterizes the anharmonicity of the trap. The dimensionless GP equations describing the dynamics of the system can be written as [31, 32].

$$\begin{aligned} (1-\gamma)i\frac{\partial\psi_1}{\partial t} &= \left[-\frac{1}{2}\nabla^2 + V + i\Omega\left(x\partial_y - y\partial_x\right) + \lambda_0|\psi|^2 + \lambda_2\left(|\psi_1|^2 + |\psi_0|^2 - |\psi_{-1}|^2\right)\right]\psi_1 \\ &\quad + \left[B(x+iy) + k\left(-i\partial_x - \partial_y\right)\right]\psi_0 + \lambda_2\psi_{-1}^{*}\psi_0^2, \end{aligned} \tag{4}$$

$$\begin{aligned} (1-\gamma)i\frac{\partial\psi_0}{\partial t} &= \left[-\frac{1}{2}\nabla^2 + V + i\Omega\left(x\partial_y - y\partial_x\right) + \lambda_0|\psi|^2 + \lambda_2\left(|\psi_1|^2 + |\psi_{-1}|^2\right)\right]\psi_0 \\ &\quad + \left[B(x-iy) + k\left(-i\partial_x + \partial_y\right)\right]\psi_1 + \left[B(x+iy) + k\left(-i\partial_x - \partial_y\right)\right]\psi_{-1} + 2\lambda_2\psi_1\psi_{-1}\psi_0^{*}, \end{aligned} \tag{5}$$

$$\begin{aligned} (1-\gamma)i\frac{\partial\psi_{-1}}{\partial t} &= \left[-\frac{1}{2}\nabla^2 + V + i\Omega\left(x\partial_y - y\partial_x\right) + \lambda_0|\psi|^2 + \lambda_2\left(|\psi_{-1}|^2 + |\psi_0|^2 - |\psi_1|^2\right)\right]\psi_{-1} \\ &\quad + \left[B(x-iy) + k\left(-i\partial_x + \partial_y\right)\right]\psi_0 + \lambda_2\psi_1^{*}\psi_0^2. \end{aligned} \tag{6}$$

where $\psi_j = N^{-1/2}a_h\Psi_j$ $(j = 0, \pm 1)$ denotes the dimensionless jth component wave function, and the total particle density is given by $|\psi|^2 = |\psi_1|^2 + |\psi_0|^2 + |\psi_{-1}|^2$, and the dimensionless external potential is $V = (r^2 + \mu r^4)/2$. Here, $\lambda_0 = 4\pi N(2a_2 + a_0)/3a_h$ and $\lambda_2 = 4\pi N(a_2 - a_0)/3a_h$ represent dimensionless density–density and spin–exchange interactions, respectively. B, k, and Ω denote dimensionless quadrupole field strength, SOC strength, and rotation frequency, respectively. That is, in the numerical calculations of our study, the length (x and y), time, energy (interaction, SOC, and rotation), and magnetic field gradient are measured in units of $\sqrt{\hbar/m\omega_{\perp}}$, $1/\omega_{\perp}$, $\hbar\omega_{\perp}$, and $\hbar\omega_{\perp}/(g_F\mu_B a_h)$, respectively.

For spin-1 BEC, the spin texture is defined as [33, 34].

$$\mathbf{S}_\alpha = \sum_{m,\ n=0,\pm1}\psi_m^{*}(f_\alpha)_{m,n}\psi_n\Big/|\psi|^2\ (\alpha = x, y, z). \tag{7}$$

The spatial distribution of the topological structure of the system is characterized by the topological charge density

$$q(r) = \frac{1}{4\pi}\mathbf{s}\bullet\left(\frac{\partial\mathbf{s}}{\partial x}\times\frac{\partial\mathbf{s}}{\partial y}\right), \tag{8}$$

with $\mathbf{s} = \mathbf{S}/|\mathbf{S}|$ and that topological charge Q is defined by

$$Q = \int q(r)dxdy. \tag{9}$$

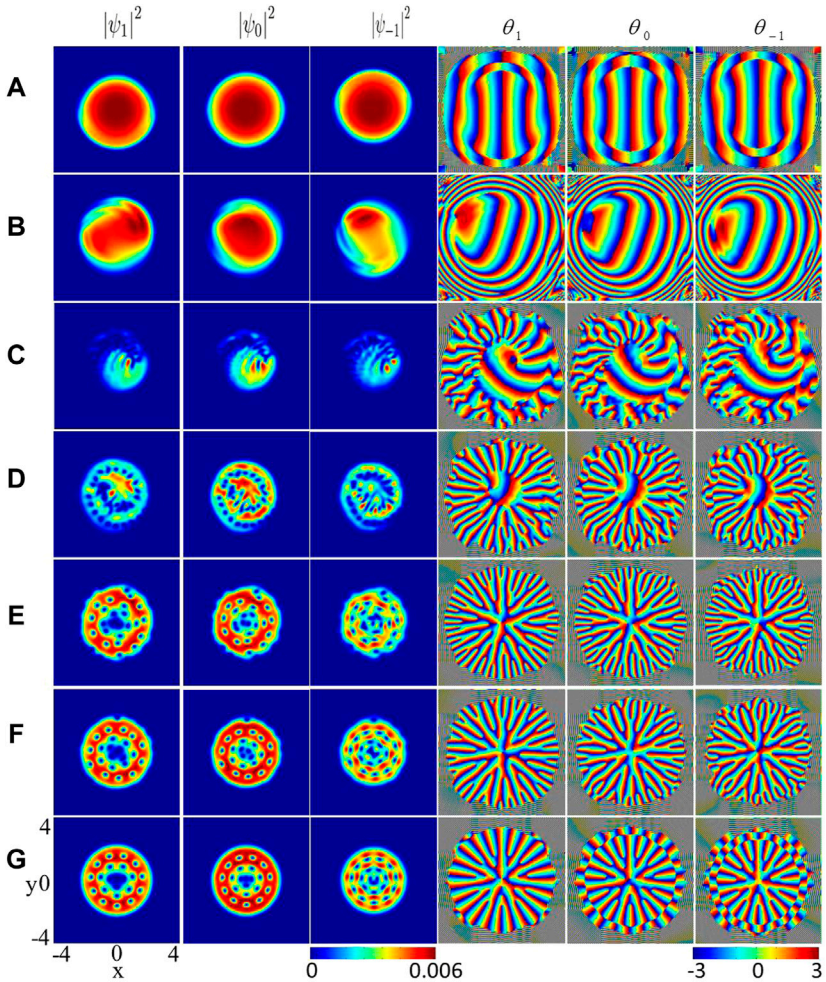

FIGURE 1 | Dynamics evolution of rotated spin-orbit-coupled spin-1 BECs. The first to the third columns are the density distributions of three components $|F = 1, m_F = 1\rangle$, $|F = 1, m_F = 0\rangle$, and $|F = 1, m_F = -1\rangle$, and the corresponding phase distributions are displayed in the fourth to the sixth columns, respectively. **(A)** Initial quantum state with SOC strength $k = 2$, **(B–G)** respective dynamic structures of $t = 0.2$, $t = 1.5$, $t = 6$, $t = 15$, $t = 25$, and $t = 600$ with the system suddenly beginning to rotate with $\Omega = 2$. The length and time are in units of a_0 and $1/\omega_\perp$, respectively.

The topological charge $|Q|$ is unchanged, no matter how one exchanges the components of the spin density vector $\mathbf{S}_x$, $\mathbf{S}_y$ and $\mathbf{S}_z$.

3 RESULTS AND DISCUSSION

In what follows, we study the dynamics of rotating spin-orbit-coupled spin-1 BECs without an in-plane gradient magnetic field and with an in-plane gradient magnetic field in an anharmonic trap. We can numerically solve the GP **Eqs. 4–6** by using the split-step Fourier method [24, 25]. First, with the imaginary-time propagation method based on the Peaceman–Rachford method [35–37], the initial quantum state of the abovementioned two cases can be obtained for $\Omega = 0$. The variation of nonzero γ does not change the dynamics of the vortex formation and the ultimate steady structure of the rotating system but only influences the relaxation time scale. In this work, we take $\gamma = 0.03$, which corresponds to a temperature of about 0.1 T_c. The relevant parameters are $\lambda_0 = 2000$ and $\lambda_2 = -100$, and the typical parameter of the anharmonic trap is chosen as $\mu = 0.5$.

3.1 Dynamics of Rotating Spin-Orbit-Coupled Spin-1 BECs in an Anharmonic Trap

It is to be noted that $|\psi_1|^2$, $|\psi_0|^2$, and $|\psi_{-1}|^2$ (the left three columns) are the density distributions of three components $m_F = 1$, $m_F = 0$, and $m_F - 1$, and the corresponding phase distributions are given by $\theta_1 = \arg\ \psi_1$, $\theta_0 = \arg\ \psi_0$, and $\theta_{-1} = \arg\ \psi_{-1}$ (the right three columns), respectively. In **Figure 1A**, we give the initial quantum state of spin-1 BECs with SOC strength $k = 2$ loaded in an anharmonic trap. The system supports an approximately disk-shaped condensate without any topological defects in each component; therefore, it presents a plane wave phase [38]. **Figures 1B–G** show the typical dynamics of the component densities and phases with the anharmonic trap beginning to

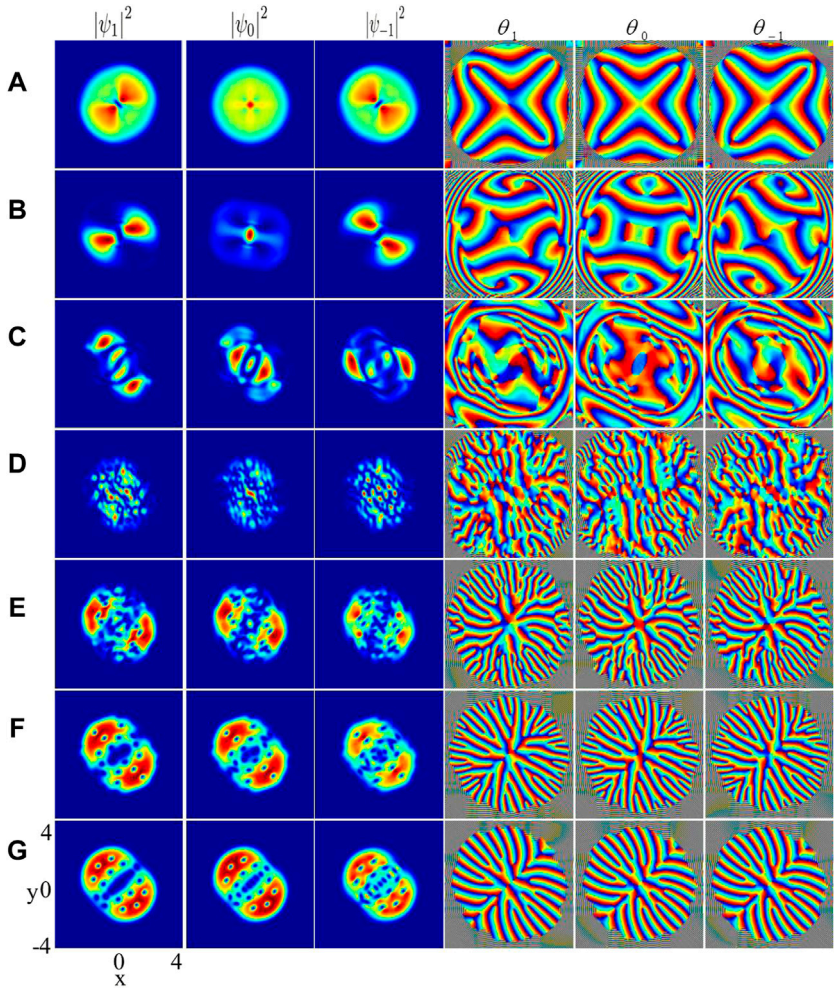

FIGURE 2 | Dynamics evolution of rotated spin-orbit-coupled spin-1 BECs with an in-plane quadrupole field. The first to the third columns are the density distributions of three components $|F = 1, m_F = 1\rangle$, $|F = 1, m_F = 0\rangle$, and $|F = 1, m_F = -1\rangle$, and the corresponding phase distributions are displayed in the fourth to the sixth columns, respectively. **(A)** Initial quantum state with SOC strength $k = 2$ and quadrupole field strength $B = 2$, **(B–G)** respective dynamic structures of $t = 0.1$, $t = 0.3$, $t = 1.3$, $t = 5$, and $t = 15$, $t = 600$ with the system suddenly beginning to rotate with $\Omega = 2$. The length and time are in units of a_0 and $1/\omega_\perp$, respectively.

rotate suddenly with $\Omega = 2$, when the system has been prepared to the initial quantum state. It is shown that during the early evolution period (see **Figure 1B**), there is a slightly turbulent oscillation in BECs, where the approximately disk-shaped densities are broken and begin to deform. Moreover, ghost vortices are formed in the boundary regions of the BECs due to the surface wave excitations [24, 27]. Then, the system reaches the minimum in the density distribution, and complex turbulent oscillations appear in the phase distributions (**Figure 1C**), which results in the surface waves propagating along the surfaces. When $t = 6$, the ghost vortex [24, 39] enters the central region of the external potential and develops into visible vortices which present irregular distributions (**Figure 1D**). With further time evolution, the component density distributions gradually become regular and the phase defects gradually gather to trap the center (**Figures 1E,F**). Eventually, the system develops into two vortex necklace structures along the azimuthal direction with an irregular density hole. In addition, the vortices in the density hole in the three components differ by one quantum number in turn (see **Figure 1G**). One of the reasons for the abovementioned density structures in **Figure 1G** is the presence of the anharmonic trap. A similar necklace structure has been found in the literature [20, 27, 40], and in the first Ref, ground states are studied in an unharmonic trap, and the latter two are dynamics in a quasicrystalline optical lattice and harmonic trap, respectively. In addition, we know that the shape of the external potential plays an important role in the dynamic properties of the BECs; for example, the system confined in a toroidal trap eventually evolved into a density hole with giant vortex structures.

3.2 Dynamics of Rotating Spin-Orbit-Coupled Spin-1 BECs With In-Plane Gradient Magnetic Field in an Anharmonic Trap

Next, we study the dynamics of rotating spin-orbit-coupled spin-1 BECs with an in-plane gradient magnetic field in an

anharmonic trap. In **Figure 2A**, we show the initial quantum state of spin-1 BECs with SOC strength $k = 2$ and in-plane quadrupole field strength $B = 2$. The vortices occur only in the central regions of the components $m_F = 1$ and $m_F = -1$, which form a polar-core vortex [41] with winding combination $\langle -1, 0, 1\rangle$, as shown in **Figure 2A**. Essentially, the polar-core vortices in **Figure 2A** are coreless vortices because there is no phase defect in the total density of the system. Our numerical simulation shows that the formation of the central polar-core vortex is relevant to the interplay between the quadrupole field and the SOC. The combined effects of the quadrupole field and the SOC generate a special saddle point structure, where the in-plane magnetization of the spin occurs in the particular magnetic field and the amplitude of the total magnetization $|\mathbf{F}|$ at the saddle point is zero. To satisfy the conservation of angular momentum, the two vortices at the center of components $m_F = 1$ and $m_F = -1$ must rotate backward, so they have opposite winding numbers. The typical dynamics of the component densities and phases after the anharmonic trap begins to rotate suddenly with $\Omega = 2$ and are given in **Figures 1B–G**. As seen from the phase distributions of **Figure 2B**, there are slightly turbulent oscillations and some ghost vortices. At the same time, the components $m_F = \pm 1$ obey anti-symmetric with a diagonal line, and the component $m_F = 0$ exists in two vortex dipoles (vortex–antivortex pairs). Then, the component densities are elongated along the diagonal line and are separated (**Figure 2C**). In addition, the central polar-core vortex and a small number of ghost vortices outside the atomic cloud (last three columns of **Figure 2B**) transform into complex turbulent oscillations in the phase distribution (last three columns of **Figure 2C**). When $t = 1.3$, the system becomes fragments and reaches the minimum in the density distributions, and the corresponding distributions present more complicated turbulence oscillations, which makes the boundary of the BECs unstable and induces surface waves propagating along the surfaces. With further time evolution, the condensates gradually split into two obvious parts about a diagonal line and the center of the system appears to dissipate (see **Figures 2E,F**). The visible vortices of the system eventually link up with each other along the principal diagonal, that is, a diagonal vortex chain, with the remaining vortices distributed symmetrically as far as possible on both sides of the diagonal line (**Figure 2G**). Physically, here the vortex chain is a result of the combined effect of SOC, in-plane quadrupole field, and rotation. The magnetic field gradient causes a magnetic force so that the condensate is difficult to concentrate at the center and is divided into two parts, and on the other hand, due to the existence of rotation, the competition among the magnetic force, SOC, and the rotation, a vortex chain appears. The vortex chain structure has been observed in the literature [42, 43], where only ground states with in-plane gradient magnetic fields are considered. The abovementioned research shows that in the dynamics, the combined effect of gradient magnetic fields, SOC, and rotation play a key role in the generation of exotic topological defects. On the experimental side, searching for novel quantum phases in this highly tunable system is still an ongoing work. Our findings will stimulate further research in searching for various novel states in spin-orbit coupled BECs subject to effective gradient fields. In addition, tunable atomic spin-orbit coupling synthesized with a modulating gradient magnetic field has been realized [44–46]

3.3 Spin Texture

The skyrmion is a type of topological soliton, which was originally suggested in nuclear physics by Skrme to elucidate baryons as a quasiparticle excitation with spins pointing in all directions to wrap a sphere [47]. A skyrmion can be viewed as the reverse of the local spin, and the spin-vector sweeps the whole unit sphere; therefore, its topological charge is $Q = 1$. As shown **Figure 3** and **Figure 4**, we display the typical transitions of the topological charge density and spin texture. Displayed in **Figures 3A,B** are the topological charge density and the spin texture, and the corresponding density and phase distributions ($t = 6$) are given in **Figure 1D**. **Figures 3C–G** represent the typical local amplifications of the spin texture in **Figure 3B**, and **Figure 3H** shows the topological charge density of $t = 11$ (**Figure 1E**). Considering the limited resolution of the texture, in **Figure 3I**, we only show the spin texture in the core region, and the typical local amplifications of the full spin texture are given in **Figures 3J–N**. Our numerical calculation shows that **Figures 3C–E** and **Figures 3J–M** denote half-antiskyrmions [21, 48] with topological charge $Q = -0.5$, and **Figures 3F,G** and **Figure 3N** present antiskyrmions with topological charge $Q = -1$, which indicates that the spin texture in the process of evolution comprises different types of half-antiskyrmions (antimerons) and antiskyrmions. Due to the transitional spin texture being unstable, we cannot determine exactly what the topological defect is. Shown in **Figures 3O,P** are the topological density and spin texture of the steady state, and the local amplifications are given in **Figures 3Q–U**, Our calculation results demonstrate that the topological defect of the central region in the green spot is a hyperbolic antiskyrmion with unit topological charge $Q = -1$. The hyperbolic skyrmion and hyperbolic half-skyrmions have been reported in the literature [21, 47–49]. The topological defect in **Figures 3Q–T** is half-antiskyrmion (antimeron) with topological charge $Q = -0.5$, where different colors of dots represent half-antiskyrmions with different shapes. As seen from **Figure 3O**, there are seven half-skyrmions around the trap center, which develop into a half-antiskyrmion necklace structure along the azimuthal direction, and the external region of the cloud is occupied by a larger half-antiskyrmion necklace comprising eleven half-antiskyrmions, that is, the half-antiskyrmion necklace consists of two concentric annular half-antiskyrmions. In short, the spin texture undergoes a transition from an irregular antimeron and antiskyrmion structures to a double half-antiskyrmion necklace structure.

Figure 4A shows the spin structure corresponding to **Figure 2A**, and it indicates that the spin of the initial state is fully magnetized into the plane and whose arrangement resembles the configuration of a quadrupole magnetic field. The center of the quadrupole magnetic field is a saddle point with the magnetic field strength being 0, which has no magnetization. However, due to the continuity of the wave function, the spin function $\mathbf{S}(\mathbf{r})$ in the center point must be continuous. If $\mathbf{S}(\mathbf{0})$ has a certain magnitude, it must point in a certain direction. However, due to the symmetry of the system, no matter $\mathbf{S}(\mathbf{0})$ choice, any direction will break the continuity of $\mathbf{S}(\mathbf{r})$ at the center point. So, $\mathbf{S}(\mathbf{0})$ can only take 0 to satisfy the continuity condition. Therefore, the components $m_F = 1$ and

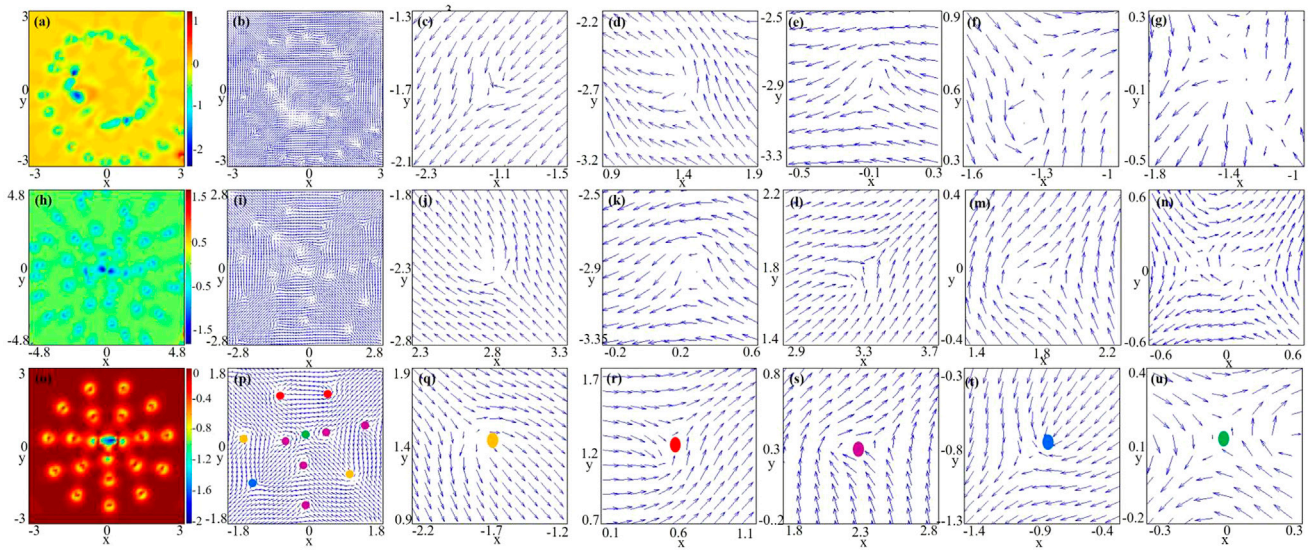

FIGURE 3 | Transition of topological charge densities and spin textures in the anharmonic trap. **(A–U)** correspond to **Figures 1D,E,G**, respectively. The left two columns represent the topological charge densities and spin texture, and the right four columns denote the local enlargements of spin textures, respectively. **(C–E)**, **(I–M)**, **(Q–T)** denote half-antiskyrmions, and **(F,G)**, **(N,U)** denote antiskyrmions. The unit length is a_0.

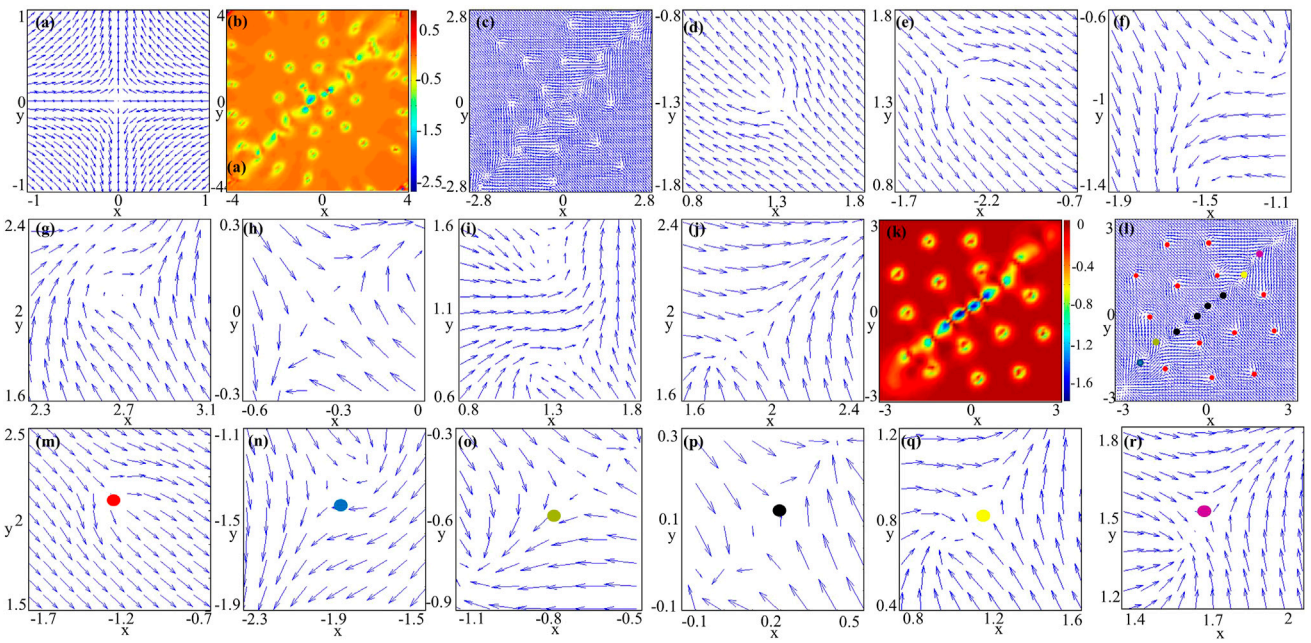

FIGURE 4 | Transition of topological charge densities and spin textures. **(A)** is the texture of **Figure 2A**. **(B–J)** and **(K–R)** correspond to **Figures 2F,G**, respectively. **(B,C)** and **(K,L)** represent the topological charge densities and spin textures, and the rest represent the local enlargements of spin textures, which denote half-antiskyrmions, respectively. The unit length is a_0.

$m_F = -1$ form a central vortex core. To satisfy the conservation of angular momentum, the two vortices at the center of $|F = 1, m_F = 1\rangle$ and $|F = 1, m_F = -1\rangle$ components must rotate in opposite directions, which forms central polar-core vortex (see **Figure 2A**). **Figures 4B,C** exhibit the topological charge density and spin texture of $t = 15$, which corresponds to **Figure 2F**. From **Figures 4D–J**, there are seven types of half-antiskyrmions with respective local topological charge $Q = -0.5$, and they seem to be forming a half-antiskyrmion chain along the diagonal. As shown in **Figures 4K,L** are the topological charge density and spin texture of the

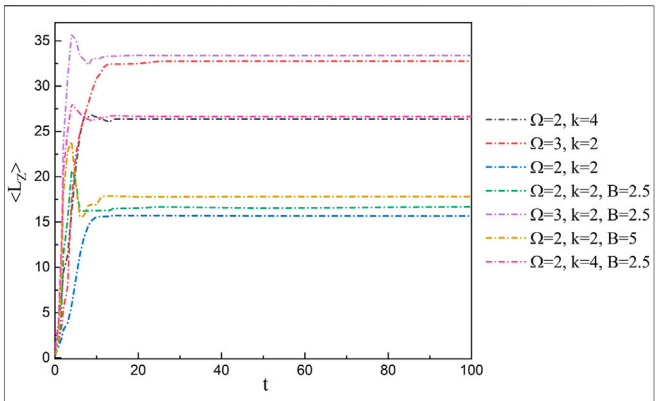

FIGURE 5 | Time evolution of the average angular momentum per atom $\langle L_z \rangle$ with $\gamma = 0.03$. Here $\langle L_z \rangle$ and t are in units of $\hbar$ and $1/\omega_\perp$, respectively.

steady state, and the local amplifications are given in **Figures 4M–R**. The topological structure of the leading diagonals is a chain comprising different kinds of half-antiskyrmions, whose respective local topological charge $Q = -0.5$. Moreover, the local topological charge in each red spot is $Q = -0.5$, which indicates that the topological structures on both sides of the leading diagonals are a symmetric half-antiskyrmion (antimeron) lattice with it. In a word, the spin texture transforms from a structure similar to a quadrupole magnetic field to a symmetric half-antiskyrmion lattice with respect to the diagonal of the half skyrmion chain. Essentially, the half-antiskyrmions (antiskyrmions) of different shapes in **Figure 3** and **Figure 4** are caused by the complicated interplay among the SOC, rotation, in-plane gradient magnetic field, and dissipation.

The dynamic process can also be characterized by the time evolution of the average angular momentum per atom $\langle L_z \rangle$, where the dependence of $\langle L_z \rangle$ on Ω, k, and B is displayed in **Figure 5**. Take the blue curve as an example, when the system suddenly begins to rotate with $\Omega = 2$, $\langle L_z \rangle$ increases rapidly with the time evolution ($0 \leq t \leq 15$), and the gradually ($15 \leq t \leq 100$) approaches a maximum value (equilibrium value). Essentially, the combined effects of the continuous input of angular momentum, quantum fluid nature, SOC, anharmonic trap, and the dissipation result in the formation of a steady vortex structure in the three components. Next, we take the green curve as an example, and as the system is rotated with $\Omega = 2$, $\langle L_z \rangle$ increases rapidly ($0 \leq t \leq 5$) and suddenly a small ($5 \leq t \leq 8$) decrease occurs and finally tends to be an equilibrium value. Compared with the former, we find that the final $\langle L_z \rangle$ is larger for the latter. That is, the combined effects of the quantum fluid nature, SOC, in-plane gradient magnetic field, and dissipation enhance the creation of vortices on the diagonal.

4 CONCLUSION

To summarize, we investigate the dynamics of rotating spin-orbit-coupled spin-1 BECs in an in-plane gradient magnetic field, which is confined in an anharmonic trap. Such a system sustains peculiar and interesting dynamic behaviors due to the multicomponent-order parameters and the interplay among the in-plane quadrupole field, SOC, rotation, and dissipation. In order to study the dynamics, the system is rotated suddenly after the system has been prepared to an initial quantum state. For the case of rotating spin-orbit-coupled spin-1 BECs, with the dynamic evolution, the system transforms from initial disk-shaped condensates to drastic turbulent oscillations and ghost vortices on the surface of the component densities due to the surface wave excitations and then to two final steady vortex necklaces along the azimuthal direction with an irregular density hole, where the vortices in the three components differ by one quantum number in turn, whereas for the case of rotating spin-orbit-coupled spin-1 BECs with in-plane gradient magnetic field, the system evolves from an initial central polar-core vortex to violent turbulent oscillations and then to a final vortex chain along the diagonal of BECs, with the remaining vortices symmetrically distributed on both sides in the individual component. Simultaneously, the corresponding spin texture experiences a structural phase transition from plane-wave phase to double half-antiskyrmion necklaces for the former case and a transition from a structure similar to a quadrupole magnetic field to a vortex chain with half-antiskyrmions on both sides. In addition, the angular momentum increases gradually and then approaches a convergent value. These interesting findings provide new understanding and exciting perspectives for ultracold atomic gases and condensed matter physics. Although it may be a challenge to implement the present system experimentally, this system is theoretically feasible and can be achieved in principle. For instance, one may consider a spin-1 ^{87}Rb BEC [44, 50] or a spin-1 ^{23}Na BEC [51]. With the ongoing development of cold-atom experimental techniques, the system may be realized in the future and its novel quantum phases and dynamic properties are expected to be observed in experiments.

DATA AVAILABILITY STATEMENT

The original contributions presented in the study are included in the article/Supplementary Material; further inquiries can be directed to the corresponding author.

AUTHOR CONTRIBUTIONS

HY: Conceptualization, Formal analysis, Data curation, and Writing—review. QZ: Formal analysis. ZJ: Investigation, Supervision, and Writing—review editing.

FUNDING

This work was supported by Shanxi Education Department Fund (2020L0546).

REFERENCES

1. Lin YJ, Jiménez-García K, Spielman IB. Spin-orbit-coupled Bose-Einstein Condensates. *Nature* 471 (2011) 83, 6.doi:10.1038/nature09887
2. Wu Z, Zhang L, Sun W, Xu XT, Wang BZ, Ji SC, et al. Realization of Two-Dimensional Spin-Orbit Coupling for Bose-Einstein Condensates. *Science* (2016) 354:83–8. doi:10.1126/science.aaf6689
3. Li JR, Lee J, Huang W, Burchesky S, Shteynas B, Top FÇ, et al. A Stripe Phase with Supersolid Properties in Spin-Orbit-Coupled Bose-Einstein Condensates. *Nature* (2017) 543:91–4. doi:10.1038/nature21431
4. Wang P, Yu ZQ, Fu Z, Miao J, Huang L, Chai S, et al. Spin-orbit Coupled Degenerate Fermi Gases. *Phys Rev Lett* (2012) 109:095301. doi:10.1103/PhysRevLett.109.095301
5. Cheuk LW, Sommer AT, Hadzibabic Z, Yefsah T, Bakr WS, Zwierlein MW. Spin-injection Spectroscopy of a Spin-Orbit Coupled Fermi Gas. *Phys Rev Lett* (2012) 109:095302. doi:10.1103/PhysRevLett.109.095302
6. Wang ZY, Cheng XC, Wang BZ, Zhang JY, Lu YH, Yi CR, et al. Realization of an Ideal Weyl Semimetal Band in a Quantum Gas with 3d Spin-Orbit Coupling. *Science* (2021) 372:271–6. doi:10.1126/science.abc0105
7. Kato YK, Myers RC, Gossard AC, Awschalom DD. Observation of the Spin Hall Effect in Semiconductors. *Science* (2004) 306:1910–3. doi:10.1126/science.1105514
8. Xiao D, Chang MC, Niu Q. Berry Phase Effects on Electronic Properties. *Rev Mod Phys* (2010) 82:1959–2007. doi:10.1103/revmodphys.82.1959
9. Qi XL, Zhang SC. Topological Insulators and Superconductors. *Rev Mod Phys* (2011) 83:1057–110. doi:10.1103/revmodphys.83.1057
10. Read N, Green D. Paired States of Fermions in Two Dimensions with Breaking of Parity and Time-Reversal Symmetries and the Fractional Quantum Hall Effect. *Phys Rev B* (2000) 61:10267–97. doi:10.1103/physrevb.61.10267
11. Zhai H. Degenerate Quantum Gases with Spin-Orbit Coupling: a Review. *Rep Prog Phys* (2015) 78:026001. doi:10.1088/0034-4885/78/2/026001
12. Sinha S, Nath R, Santos L. Trapped Two-Dimensional Condensates with Synthetic Spin-Orbit Coupling. *Phys Rev Lett* (2011) 107:270401. doi:10.1103/physrevlett.107.270401
13. Jiang X, Fan Z, Chen Z, Pang W, Li Y, Malomed BA. Two-dimensional Solitons in Dipolar Bose-Einstein Condensates with Spin-Orbit Coupling. *Phys Rev A* (2016) 93:023633. doi:10.1103/physreva.93.023633
14. Poon TFJ, Liu XJ. Quantum Spin Dynamics in a Spin-Orbit-Coupled Bose-Einstein Condensate. *Phys Rev A* (2016) 93:063420. doi:10.1103/physreva.93.063420
15. Kartashov YV, Konotop VV. Solitons in Bose-Einstein Condensates with Helicoidal Spin-Orbit Coupling. *Phys Rev Lett* (2017) 118:190401. doi:10.1103/physrevlett.118.190401
16. Liu CF, Juzeliūnas G, Liu WM. Spin-orbit Coupling Manipulating Composite Topological Spin Textures in Atomic-Molecular Bose-Einstein Condensates. *Phys Rev A* (2017) 95:023624. doi:10.1103/physreva.95.023624
17. Yang S, Wu F, Yi W, Zhang P. Two-body Bound State of Ultracold Fermi Atoms with Two-Dimensional Spin-Orbit Coupling. *Phys Rev A* (2019) 100:043601. doi:10.1103/physreva.100.043601
18. Wang JG, Li YQ. Vortex Lattices in a Rotating Spin-Orbit Coupled Spin-1/2 Bose-Einstein Condensates with Spatially Modulated Nonlinear Interaction. *Results Phys* (2020) 17:103099. doi:10.1016/j.rinp.2020.103099
19. Fetter AL, Jackson B, Stringari S. Rapid Rotation of a Bose-Einstein Condensate in a Harmonic Plus Quartic Trap. *Phys Rev A* (2005) 71:013605. doi:10.1103/physreva.71.013605
20. Su N, Wang Q, Hu J, Su X, H WL. Topological Defects in Rotating Spin-Orbit-Coupled Dipolar Spin-1 Bose-Einstein Condensates. *J Phys B* (2020) 53:215301. doi:10.1088/1361-6455/abb031
21. Shi CX, Wen L, Wang Q, Yang H, Wang H. Topological Defects of Spin-Orbit-Coupled Bose-Einstein in a Rotating Anharmonic Trap. *J Phys Soc Jpn* (2018) 87:094003. doi:10.7566/jpsj.87.094003
22. Qu C, Hamner C, Gong M, Zhang C, Engels P. Observation of Zitterbewegung in a Spin-Orbit-Coupled Bose-Einstein Condensate. *Phys Rev A* (2013) 88:021604. doi:10.1103/physreva.88.021604
23. Dong Y, Dong L, Gong M, Pu H. Dynamical Phases in Quenched Spin-Orbit-Coupled Degenerate Fermi Gas. *Nat Commun* (2015) 6:6103. doi:10.1038/ncomms7103
24. Wen L, Xiong H, Wu B. Hidden Vortices in a Bose-Einstein Condensate in a Rotating Double-Well Potential. *Phys Rev A* (2010) 82:053627. doi:10.1103/physreva.82.053627
25. Wen LH, Luo XB. Formation and Structure of Vortex Lattices in a Rotating Double-Well Bose-Einstein Condensate. *Laser Phys Lett* (2012) 9:618. doi:10.7452/lapl.201210044
26. Kasamatsu K, Tsubota M, Ueda M. Nonlinear Dynamics of Vortex Lattice Formation in a Rotating Bose-Einstein Condensate. *Phys Rev A* (2003) 67:033610. doi:10.1103/physreva.67.033610
27. Wang QB, Hu JG, Su XH, Wen LH. Dynamics of Rotating Spin-Orbit-Coupled Bose-Einstein Condensates in a Quasicrystalline Optical Lattice. *Results Phys* (2021) 20:103755. doi:10.1016/j.rinp.2020.103755
28. Tsubota M, Kasamatsu K, Ueda M. Vortex Lattice Formation in a Rotating Bose-Einstein Condensate. *Phys Rev A* (2002) 65:023603. doi:10.1103/physreva.65.023603
29. Kawaguchi Y, Ueda M. Spinor Bose-Einstein Condensates. *Phys Rep* (2012) 520:253. doi:10.1016/j.physrep.2012.07.005
30. Stamper-Kurn DM, Ueda M. Spinor Bose Gases: Symmetries, Magnetism, and Quantum Dynamics. *Rev Mod Phys* (2013) 85:1191. doi:10.1103/revmodphys.85.1191
31. Martikainen JP, Collin A, Suominen KA. Coreless Vortex Ground State of the Rotating Spinor Condensate. *Phys Rev A* (2002) 66:053604. doi:10.1103/physreva.66.053604
32. Lovegrove J, Borgh MO, Ruostekoski J. Energetically Stable Singular Vortex Cores in an Atomic Spin-1 Bose-Einstein Condensate. *Phys Rev A* (2012) 86:013613. doi:10.1103/physreva.86.013613
33. Mizushima T, Kobayashi N, Machida K. Coreless and Singular Vortex Lattices in Rotating Spinor Bose-Einstein Condensates. *Phys Rev A* (2004) 70:043613. doi:10.1103/physreva.70.043613
34. Kasamatsu K, Tsubota M, Ueda M. Spin Textures in Rotating Two-Component. *Bose-Einstein condensates* (2005) 71:043611. doi:10.1103/physreva.71.043611
35. Zhang Y, Mao L, Zhang C. Mean-field Dynamics of Spin-Orbit Coupled Bose-Einstein Condensates. *Phys Rev Lett* (2012) 108:035302. doi:10.1103/PhysRevLett.108.035302
36. Peaceman DW, Rachford HH. The Numerical Solution of Parabolic and Elliptic Differential Equations. *J Soc Ind Appl Math* (1955) 3:28. doi:10.1137/0103003
37. Wen L, Qiao Y, Xu Y, Mao L. Structure of Two-Component Bose-Einstein Condensates with Respective Vortex-Antivortex Superposition States. *Phys Rev A* (2013) 87:033604. doi:10.1103/physreva.87.033604
38. Wang C, Gao C, Jian CM, Zhai H. Spin-orbit Coupled Spinor Bose-Einstein Condensates. *Phys Rev Lett* (2010) 105:160403. doi:10.1103/physrevlett.105.160403
39. Yang H, Wang Q, Su N, Wen L. Topological Excitations in Rotating Bose-Einstein Condensates with Rashba-Dresselhaus Spin-Orbit Coupling in a Two-Dimensional Optical Lattice. *Eur Phys J Plus* (2019) 134:589. doi:10.1140/epjp/i2019-12988-y
40. Liu CF, M LW. Spin-orbit-coupling-induced Half-Skyrmion Excitations in Rotating and Rapidly Quenched Spin-1 Bose-Einstein Condensates. *Phys Rev A* (2012) 86:033602. doi:10.1103/physreva.86.033602
41. Sadler LE, Higbie JM, Leslie SR, Vengalattore M, Stamper-Kurn DM. Spontaneous Symmetry Breaking in a Quenched Ferromagnetic Spinor Bose-Einstein Condensate. *Nature* (2006) 443:312. doi:10.1038/nature05094
42. Wang JG, Yang SJ. Ground-state Phases of Spin-Orbit-Coupled Spin-1 Bose-Einstein Condensate in a Plane Quadrupole Field. *J Phys.:Condens Matter* (2018) 30:295404. doi:10.1088/1361-648x/aacc42
43. Li J, Liu WM. Ground State of Spin-Orbit Coupled Rotating Two-Component Bose-Einstein Condensate in Gradient Magnetic Field. *Acta Phys Sin* (2018) 67:110302. doi:10.7498/aps.67.20180539
44. Luo X, Wu L, Chen J, Guan Q, Gao K, Xu Z, et al. Tunable Atomic Spin-Orbit Coupling Synthesized with a Modulating Gradient Magnetic Field. *Sci Rep* (2016) 6:18983. doi:10.1038/srep18983
45. Xu ZF, You L, Ueda M. Atomic Spin-Orbit Coupling Synthesized with Magnetic-Feld-Gradient Pulses. *Phys Rev A* (2013) 87:063634. doi:10.1103/physreva.87.063634

46. Anderson BM, Spielman IB, Juzeliunas G. Magnetically Generated Spin-Orbit Coupling for Ultracold Atoms. *Phys Rev Lett* (2013) 111:125301. doi:10.1103/physrevlett.111.125301
47. Skyrme THR. A Unified Field Theory of Mesons and Baryons. *Nucl Phys* (1962) 31:556. doi:10.1016/0029-5582(62)90775-7
48. Kasamatsu K, Tsubota M, Ueda M. Vortex Molecules in Coherently Coupled Two-Component Bose-Einstein Condensates. *Phys Rev Lett* (2004) 93:250406. doi:10.1103/physrevlett.93.250406
49. Liu CF, Fan H, Zhang YC, Wang DS, Liu WM. Circular-hyperbolic Skyrmion in Rotating Pseudo-spin-1/2 Bose-Einstein Condensates with Spin-Orbit Coupling. *Phys Rev A* (2012) 86:053616. doi:10.1103/physreva.86.053616
50. Campbell DL, Price RM, Putra A, Valdés-Curiel A, Trypogeorgos D, Spielman IB. Magnetic Phases of Spin-1 Spin-Orbit-Coupled Bose Gases. *Nat commun.* (2016) 7:10897. doi:10.1038/ncomms10897
51. Stenger J, Inouye S, Stamper-Kurn DM, Miesner HJ, Chikkatur AP, Ketterle W. Spin Domains in Ground-State. *Bose-Einstein condensates* (1998) 396:345. doi:10.1038/24567

Conflict of Interest: The authors declare that the research was conducted in the absence of any commercial or financial relationships that could be construed as a potential conflict of interest.